ISSN XXXX XXXX © 2017 IJESC

Research Article Volume 7 Issue No.7

Analysis of Electron Charge Density of $BaTiO_3$ and $CaTiO_3$ using Multipole Analysis Method

S.J.Anto Juliyana[1], M.Revathi[2]
M.Phil Student[1], Research supervisior[2]
Department of Physics
PRIST University, Madurai Campus, India

Abstract:
The electronic charge density analysis of $CaTiO_3$ and $BaTiO_3$ has been accomplished by analyzing the powder x-ray diffraction data using a versatile method called multipole analysis method. The accuracy of the data is good enough for the chosen study reflected by the low reliability indices obtained after refinement, the charge density map along with static and dynamic deformation maps have shown the type of bonding involved in the material. The final analysis of the electronic charge density shows the ionic bonding between the Ca and O atoms and between Ba and Ti atoms. Covalent bond is found to exist between Ti and O atoms. The method of multipole analysis has been used for the first time for the chosen material.

Keywords: charge density, diffraction, multipole analysis, indicies, refinement

I. INTRODUCTION

A crystal is the one in which the atoms or molecules are arranged periodically. Within a crystal, many identical parallelepiped unit cells, each containing a group of atoms, are packed together to fill all space. In scientific nomenclature, the term crystal is usually short for single crystal, a single periodic arrangement of atoms. Most gems are single crystals. However, many materials are polycrystalline, consisting of many small grains, each of which is a single crystal. Crystalline substances are grouped, according to the type of symmetry they display, into 32 classes. A crystalline sample is by definition periodic; a crystal is composed of a unit cell repeated over and over in three independent directions. Such periodic systems have a Fourier transform that is concentrated at periodically repeating points in reciprocal space known as Bragg peaks; the Bragg peaks correspond to the reflection spots observed in the diffraction image.

Experimental Method

There are two practical variants of the Laue method, the back-reflection and the transmission Laue method. Back-reflection Laue experimental arrangement is shown below.

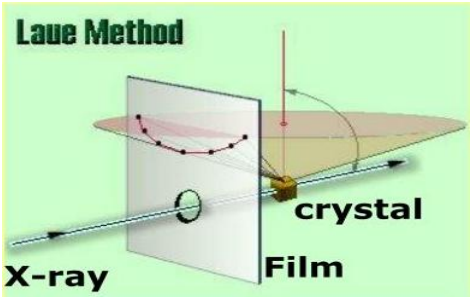

Figure .1. Back-reflection Laue experimental arrangement

In the back-reflection method, the film is placed between the x-ray source and the crystal. The beams which are diffracted in a backward direction are recorded. One side of the cone of Laue reflections is defined by the transmitted beam. The film intersects the cone, with the diffraction spots generally lying on an hyperbola.

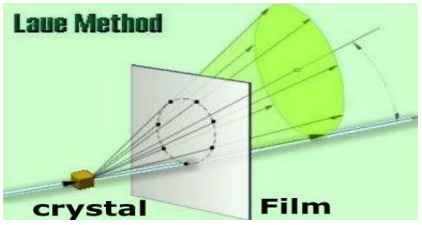

Figure. 2.Transmission Laue experimental arrangement

In the transmission Laue method, the film is placed behind the crystal to record beams which are transmitted through the crystal. One side of the cone of Laue reflections is defined by the transmitted beam. The film intersects the cone, with the diffraction spots generally lying on an eclipse

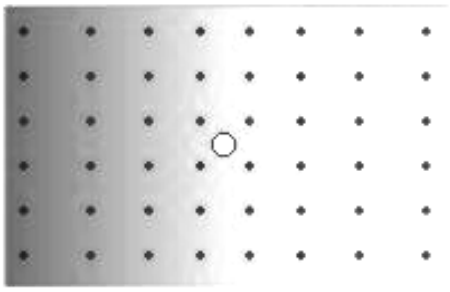

Figure. 3. Back-reflection Laue photograph

In the rotating crystal method, a single crystal is mounted with an axis normal to a monochromatic x-ray beam. A cylindrical film is placed around it and the crystal is rotated about the chosen axis.As the crystal rotates, sets of lattice planes will at some point make the correct Bragg angle for the monochromatic incident beam, and at that point a diffracted beam will be formed. The reflected beams are located on the surface of imaginary cones. When the film is laid out flat, the diffraction spots lie on.

Introduction to Charge density

Since the lattice has a periodicity, the electron density is also considered to behave as a periodic function. The number of electrons in any volume element dV is $\rho(x,y,z)\,dV$. In a X-ray scattering experiment, the wavelet scattered by this element is

$$\rho(x,y,z)\exp[-2\pi i(hx + ky + lz)]dV \quad \ldots (1)$$

The resultant sum of contributions from all the elements in the unit cell, i.e., the integral over its volume gives

$$F_{hkl} = \int \rho(x, y, z) \exp[-2\pi i(hx + ky + lz)]dV \quad \ldots (2)$$

The structure factor is considered as a resultant of adding the scattered waves in the direction of the hkl reflection from the atoms in the unit cell. This approach was based on the assumption that the scattering power of the electron cloud surrounding each atom could be equated to that of the proper number of electrons concentrated at the atomic centre. But the structure factor may equally well be considered as the sum of the wavelets scattered from all the infinitesimal elements of electron density in a unit cell, with no assumptions being made about the distribution of this density. The electron density ρ(r) is defined as the number of electrons per unit volume. The magnitude of individual structure factors are calculated as the square-root of the measured diffraction intensity and their phases are determined by solving the structure. The interpretation is described as a model, which is improved by least-squares refinement based on the structure factors. The electron density can then be calculated as a Fourier summation of phased structure factors. Intensities of diffracted X-rays are due to interference effects of X-rays scattered by all the different atoms in the structure. The diffraction pattern is the Fourier transform of the crystal structure, corresponding to the pattern of waves scattered from an incident X-ray beam by a single crystal; it can be measured by experiment (only partially, because the amplitudes are obtainable from the directly measured intensities via a number of correction, but the relative phases of the scattered waves are lost), and it can be calculated (giving both amplitudes and phases) for a known structure. In turn, the crystal structure is the Fourier transform of the diffraction pattern and is expressed in terms of electron density distribution concentrated in atoms; it cannot be measured by direct experiment, because the scattered X-rays cannot be refracted by lenses to form an image as done with light in an optical microscope, and it cannot be obtained directly by calculation, because the required relative phases of the waves are unknown. We can calculate the electron density distribution given a set of structure factors, using the Fourier series.

II. POWDER DIFFRACTION

Powder diffraction is a scientific technique using X-Ray or neutron diffraction on powder or microcrystalline samples for structural characterization of materials. Ideally, every possible crystalline orientation is represented equally in the sample, leading to smooth diffraction rings around the beam axis rather than the discrete Laue spotsobserved for single crystal diffraction. In practice, it is sometimes necessary to rotate the sample orientation to eliminate the effects of texturing and achieve true randomness. The dedicated machine to perform such measurements is called a powder diffractometer.The great advantages of the technique are simplicity of sample preparation, rapidity of measurement, a better representation of some real materials, and the ability to analyze mixed phases.

Powder Refinement: Rietveld Method

The Rietveld method (Rietveld, 1967; Rietveld, 1969) is a technique for refining structure parameters (fractional coordinates, isotropic/anisotropic atomic displacement parameters, and occupation factors, magnetic moments, etc.) and lattice parameters directly from whole powder diffraction patterns without separating reflections. This method is very useful (i) when single crystals cannot be grown at all, (ii) when only twinned samples can be prepared and (iii) when physical and/or chemical properties of single-crystal forms differ from those of polycrystalline ones. Rietveld refinement is used as the last process of ab initio structure analysis. Rapid advances in high-resolution transmission electron microscopy (HRTEM) have made it easier to observe crystal-structure images. HRTEM images correspond to Fourier maps in X-ray crystal analysis, serving to construct initial structural models for Rietveld refinement.

Electronic charge density estimation

Fourier Method

Any well-behaved function can be represented by means of suitable series of trigonometric terms called Fourier series. We can imagine the unit cell is divided into small volumes dV in which there are ρ(r)dV number of electrons.The scattered amplitude from such a small volume will be ρ(r)dV times as much that from an electron at the same position. From this we find the total scattered amplitude from the distribution of electron density ρ(r).

F(H) can be expressed in terms of density ρ(r) as

$$F(H) = \int \rho(r) \exp(2\pi i H.r)\, dV \quad ..(3)$$

The inverse fourier transform of this gives the electron density

$$\rho(r) = \int F(H) \exp(-2\pi i H.r)\, dV = \frac{1}{V} F(H) \exp(-2\pi i H.r) \quad \ldots(4)$$

Multipole Density Formalism

According to this model, the charge density in a crystal is written as the superposition of harmonically vibrating aspherical atomic density distribution convolving with the Gaussian thermal displacement distribution as [Hansen and Coppens, 1978].

$$\rho(r) = \sum_{k}^{atoms} \rho_k(\vec{r} - \vec{r}_k - \vec{u}) \otimes t_k(\vec{u}) \qquad \ldots. (5)$$

where $t_k(\vec{u})$ is the Gaussian term and $\otimes$ indicates a convolution. The atomic charge density is then defined as

$$\rho_{at}(\mathbf{r}) = P_c \rho_{core}(r) + P_v \kappa^3 \rho_{valence}(\kappa r) + \sum_{l=0}^{l_{max}} \kappa'^3 R_l(\kappa' r) \sum_{m=0}^{l} P_{lm\pm} d_{lm\pm}(\theta, \phi)$$

$\ldots(6)$

The advantages of multipole model are listed below:

(i) Experimental noise is not fitted by the model functions and therefore effectively filtered out.

(ii) Thermal motion is treated separately and deconvoluted from the final result

(iii) The resulting static density provides an effective level of comparison with theoretical results.

Alternate models like “bond charge models” and “orbital based algorithms” are not competent enough to the present multipole model

III. RESULT AND DISCUSSION

DATA REFINEMENT

The Powder data measured for the chosen samples $BaTiO_3$ and $CaTiO_3$ were measured from 2θ = 15° to 120° in steps of 0.02. The wavelength used for the experiment is CuK_α, for which λ=1.54051Å. Graphite is used as the monochromatic set perpendicularly to the line of beam with the glancing angle of 3.135. The structural, profile, charge density parameters were refined in the same order. Anisotropic strain broadening with respect to the strain axis (0,0,1) is also applied for refining the profile. The cell parameters were initially taken as 3.803Å for $CaTiO_3$, 4.0093 for $BaTiO_3$. The Powder data measured for the chosen samples $BaTiO_3$ and $CaTiO_3$ were measured from 2θ =

15° to 120° in steps of 0.02. The wavelength used for the experiment is CuK_{α}, for which λ=1.54051Å. Graphite is used as the monochromator set perpendicularly to the line of beam with the glancing angle of 3.135. The structural, profile, charge density parameters were refined in the same order. Anisotropic strain broadening with respect to the strain axis (0,0,1) is also applied for refining the profile. The cell parameters were initially taken as 3.803Å for $CaTiO_3$, 4.0093 for $BaTiO_3$.The atomic scattering factor for the atoms involved was chosen from sinθ/λ = 0 in steps of 0.05 is given below.

17.9999	17.7156	16.9165	15.7431	14.3743	12.97821	11.6796	10.5496
9.6119	8.8572	8.2579	7.7799	7.3896	7.0587	6.7649	6.4923
6.2304	5.9730	5.7168	5.4612	5.2065	4.9542	4.7058	4.4633
4.2282	4.0019	3.7857	3.5804	3.3866	3.2045	3.0343	2.8759
2.7290	2.5932	2.4681	2.3531	2.2475	2.1509	2.0626	1.9819
1.9082	1.8410	1.7797	1.7237	1.6726	1.6258	1.5830	1.5438
1.5077	1.4745	1.4438	1.4153	1.3888	1.3641	1.3410	1.3192
1.2986	1.2791	1.2605	1.2427	1.2256	1.2091	1.1932	1.1777
1.1627	1.1479	1.1335	1.1193	1.1054	1.0917	1.0781	1.0647
1.0514	1.0382	1.0252	1.0122	0.9993	0.9866	0.9738	0.9612
0.9487	0.9362	0.9238	0.9114	0.8992	0.8870	0.8749	0.8629
0.8509	0.8390	0.8273	0.8156	0.8040	0.7925	0.7811	0.7698
0.7586	0.7475	0.7365	0.7256	0.7149	0.7042	0.6937	0.6832
0.6729	0.6627	0.6526	0.6427	0.6328	0.6231	0.6135	0.6041
0.5947	0.5855	0.5764	0.5674	0.5585	0.5498	0.5412	0.5327

Table 1

18.0001	17.7876	17.1802	16.6525	15.1343	13.9212	12.7191	11.6004
10.6080	9.7586	9.0494	8.4658	7.9869	7.5904	7.2554	6.9640
6.7017	6.4577	6.2243	5.9963	5.7708	5.5463	5.3226	5.1001
4.8796	4.6622	4.4491	4.2415	4.0404	3.8466	3.6608	3.4837
3.3155	3.1564	3.0066	2.8660	2.7343	2.6115	2.4971	2.3909
2.2924	2.2012	2.1169	2.0391	1.9673	1.9011	1.8402	1.7840
1.7322	1.6845	1.6404	1.5998	1.5622	1.5274	1.4951	1.4651
1.4372	1.4111	1.3867	1.3638	1.3422	1.3219	1.3026	1.2842
1.2667	1.2499	1.2338	1.2183	1.2033	1.1888	1.1747	1.1609
1.1474	1.1343	1.1213	1.1086	1.0960	1.0836	1.0714	1.0593
1.0473	1.0354	1.0236	1.0119	1.0002	0.9887	0.9772	0.9658
0.9544	0.9431	0.9319	0.9207	0.9096	0.8985	0.8875	0.8766
0.8657	0.8549	0.8442	0.8335	0.8229	0.8124	0.8019	0.7915
0.7812	0.7710	0.7609	0.7508	0.7409	0.7310	0.7212	0.7115
0.7019	0.6924	0.6829	0.6736	0.6644	0.6552	0.6462	0.6372
0.6284							

Table.2. Atomic scattering factors for core of Ti atom for sinθ/λ in steps of 0.05

2.0000	1.9980	1.9920	1.9820	1.9682	1.9508	1.9298	1.9055
1.8782	1.8480	1.8151	1.7799	1.7426	1.7034	1.6627	1.6206
1.5774	1.5334	1.4888	1.4438	1.3986	1.3535	1.3085	1.2639
1.2197	1.1762	1.1334	1.0914	1.0503	1.0101	0.9710	0.9330
0.8961	0.8603	0.8256	0.7921	0.7598	0.7286	0.6985	0.6696
0.6418	0.6150	0.5894	0.5648	0.5411	0.5185	0.4968	0.4761
0.4562	0.4372	0.4190	0.4016	0.3850	0.3691	0.3539	0.3393
0.3254	0.3122	0.2995	0.2874	0.2758	0.2648	0.2542	0.2441
0.2344	0.2252	0.2164	0.2080	0.1999	0.1922	0.1849	0.1778
0.1711	0.1646	0.1585	0.1526	0.2569	0.1415	0.1363	0.1314
0.1266	01221	0.1177	0.1136	0.1096	0.1057	0.1020	0.0985
0.0951	0.0919	0.0887	0.0857	0.0829	0.0801	0.0775	0.0749
0.0725	0.0701	0.0678	0.0657	0.0636	0.0615	0.0596	0.0577
0.0559	0.0542	0.0525	0.0509	0.0494	0.0479	0.0465	0.0451
0.0438	0.0425	0.0412	0.0400	0.0389	0.0377	0.0367	0.0356
0.0346							

Table. 3. Atomic scattering factors for core of O atom for sinθ/λ in steps of 0.05

56.0000	55.9250	55.7030	55.3500	54.8880	54.3450	53.7430	53.1060
52.4500	51.7860	51.1220	50.4600	49.8020	49.1460	48.4920	47.8390
47.1860	46.5330	45.8820	45.2320	44.5860	43.3090	42.0640	41.4560
40.8590	39.7020	38.5980	37.5460	36.5450	36.0630	3505930	34.6850
33.8180	32.9860	32.1870	31.7980	31.4150	30.6700	29.9480	28.2380
26.6520	25.1890	23.8510	21.5470	19.7010	18.2240	17.0080	15.9530
14.9880	14.0670	13.1750	12.3050	11.4610	10.6610	9.9070	9.2130
6.7040							

Table.4. Atomic scattering factors for Ba atom for sinθ/λ in steps of 0.05

The position of the atoms were taken as shown below

Atom	x	y	z
Ca	0.5	0.5	0.5
Ti	0.0	0.0	0.0
O	0.5	0.0	0.0

Table.5. The positions of the atoms in $CaTiO_3$

Atom	x	y	z
Ba	0.0	0.0	0.0
Ti	0.5	0.5	0.5
O	0.5	0.0	0.5

Table. 6. The positions of the atoms in $BaTiO_3$

a	3.802953	4.009279
b	3.802953	4.009279
c	3.802953	4.009279
α	90.0000	90.00000
β	90.0000	90.00000
γ	90.0000	90.00000
Volume	55.00002	64.44642
Density	4.103385	6.007088
G_U	-4.173611	-5.614080
G_V	4.164661	5.099857
G_W	8.368809	8.336533
L_X	5.435472	5.393133
L_{Xe}	-0.115615	-0.197919
L_Y	-2.970687	-2.658643
L_{Ye}	0.810183	0.704287
Asym 1	0.005601	-0.015744
Asym 2	-0.012207	0.027698
Asym 3	0.000453	0.000048
Asym 4	-0.000859	-0.000291
Pref 1	0.963236	0.963582

The structural and refine parameters resulted in the following tables **TABLE 7:** Using the structure factors refined after multipole analysis used for constructing the charge density maps. The refined profiles along with the error bar and respective Bragg position are shown in fig

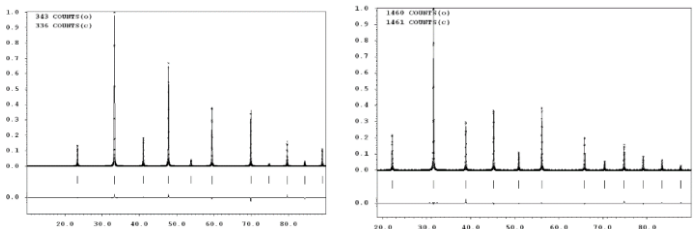

Figure.4. (a) Refined powder profile of $CaTiO_3$ (b) Refined powder profile of $BaTiO_3$

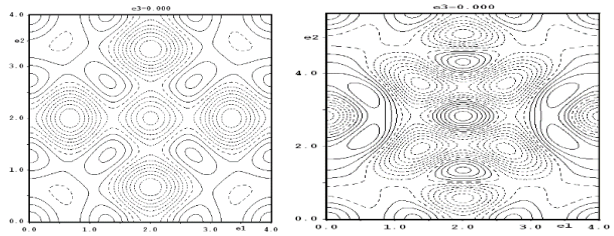

(c)Difference Fourier density map along [100] (d) Difference Fourier density map along [100]

Charge density distribution in $CaTiO_3$

The Charge density distribution using the observed structure factor was constructed in an unit cell which resulted in the maximum density of 32.23e/Å^3 which coincided with the position of Ti atom. The minimum density of -3.61e/Å^3 was observed. The charge density map constructed upon (100) plane and (110) plane as shown in the figure

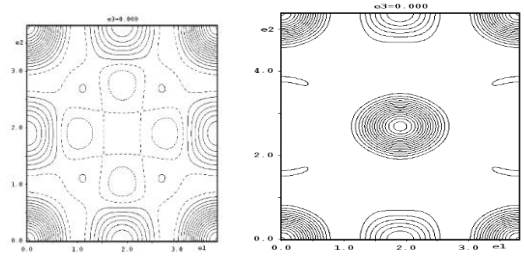

Figure.5. (a) Charge density along [100] (b)Charge density along [110]

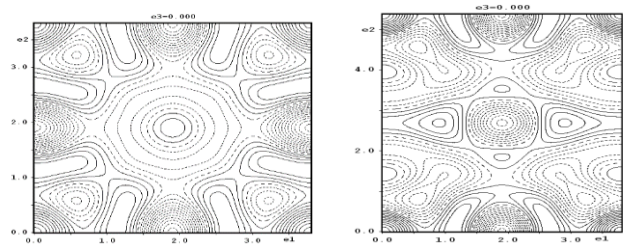

(c)Difference Fourier density map along [100] (d) Difference Fourier density map along [100]

Charge density distribution in $BaTiO_3$

The Charge density distribution using the observed structure factor were constructed in a unit cell which resulted in the maximum density of 94.31e/Å^3 which coincided with the position of Ti atom. The minimum density of -6.77e/Å^3 was observed .The charge density map constructed upon (100) plane and (110) plane as shown in fig.

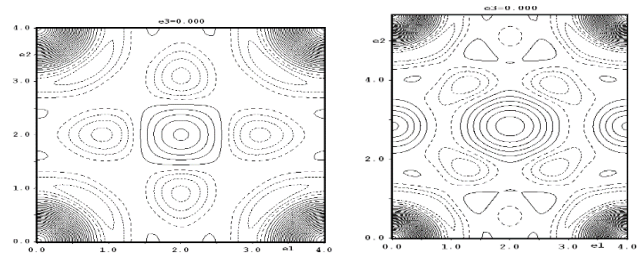

Figure.6. (a)Charge density map along [100] (b) Charge density map along [110]

The maximum density and the minimum density in the whole of the unit cell is found to be 0.34 and -0.43 e/ Å^3 respectively. The maps upon (100) & (110) plane were given

IV. CONCLUSION

The charge density map for Calcium Titanate and Barium Titanate have been constructed for the first time using powder diffraction data analyzed with the help of Rietveld refinement and multipole analysis. The reliability indices obtained from the refinement analysis have shown that the data are highly reliable for the chosen charge density analysis. The multipole analysis yields the population parameters that are in line with the theoretical expectations. The charge density maps and the deformation maps gave a clear understanding of the bonding exist in the material. The topological analysis of the charge density gave an insight on different critical points exist in the unit cell. In all the analysis done in the present work has given a new dimension in the understanding of charge density in Calcium Titanate and Barium Titanate.

V. REFERENCES

[1].Arfken G., *Mathematical Methods for Physicists*, 2nd ed., Academic Press: New York, London, (1970).

[2].Bader R. F. W. and Bedddal P. M., J. *Chem. Phys.***56** (1972) 3320.

[3].Bader, R. F.W., *Atoms in Molecules: A Quantum theory, International Series of Monographs on Chemistry*, No. **22**, Clarendon press, oxford Science Publications: Oxford, New York, (1990).

[4].Becke A., *Phys. Rev. A* **38 (**1988) 3098.

[5].Becke A.D. and Edgecombe, K.E., *J. Chem. Phys*. **92** (1990) 5397.

[6].Bentley J., and Stewart R. F., *Acta. Cryst.***A30** (1974) 60.

[7].Brown A. S., and Spackman M. A., *ActaCryst*. **A47** (1991) 21.

[8].Clementi E., and Raimondi D. L., *J. Chem. Phys.***38** (1963) 2686.

[9].Clementi E., and Roetti C., *At. Data Nucl. Data Tables.***14** (1974) 177.

[10].Condon E. V., andShortley G. H., *The Theory of Atomic Spectra*, Cambridge University Press: London, New York, (1957).

[11].Collins D.M. *Nature.***298** (1982) 49.

[12].Coppens P., X-ray Charge Densities and Chemical Bonding, International Union of Crystallography, Oxford University Press, New York, 1997.

[13].Coppens P., Guru Row T. N., Leung P., Stevens E. D., Becker P. J., and Yang Y. W., *Actacryst.***A35** (1979) 63.

[14].Dawson B., *Proc. R. Soc. Lond., Ser.A.*, **298** (1967) 225, 264.

[15].Deutsch M., *Phys. Rev. B***45** (1992) 646.

[16].De Marco J. J. and Weiss, *R. J., Phys. Rev. A***137** (1965) 1869.

[17].Dollase, W. A. *J. Appl. Crystallogr*., **19** (1986) 267.

[18].Gull S. F., and Daniel G. J., *Nature*, **272** (1978) 686.

[19].Hansen, N. K., and Coppens, P., *ActaCryst*. **A34** (1978) 909.

[20].Izumi, F. (1993). "The Rietveld Method," ed. by R. A. Young, Oxford University Press, Oxford, Chap. 13.

[21]."International Tables for Crystallography," Vol. C (1992). Kluwer, Dordrecht, pp. 391Ð399.

[22]."International Tables for Crystallography," Vol. C (1992a). Kluwer, Dordrecht, pp. 219Ð 222 and pp. 384Ð391.

[23].International Tables for X-ray Crystallography, The Kynoch press, Birmingam, England, 1974.

[24].International Tables for Crystallography, The Kynoch press, Birmingam, England, 1992.

[25].Jaynes E. T., *IEEE Trans. Syst. Sci. Cybern*. **SSC-4** (1968) 227.

[26].Kohn W., and Sham L.J., *Phys. Rev*. **140** (1965) A1133.